2019 International Conference on Robotics and Automation (ICRA)
Palais des congres de Montreal, Montreal, Canada, May 20-24, 2019

Retrieval of magnetic medical microrobots from the bloodstream

V. Iacovacci, *Member, IEEE*, L. Ricotti, *Member, IEEE,* G. Signore, F. Vistoli, E. Sinibaldi, *Member, IEEE*, and A. Menciassi, *Senior Member, IEEE*

***Abstract*—Untethered magnetic microrobots hold the potential to penetrate hard-to-reach areas of the human body and to perform therapy in a controlled way. In the past decade, impressive advancements have been made in this field but the clinical adoption of magnetoresponsive microrobots is still hampered by safety issues. A tool appointed for magnetic microrobots retrieval within body fluids could enable a real paradigm change, fostering their clinical translation.**

By starting from the general problem to retrieve magnetic microrobots injected into the bloodstream, the authors introduce a magnetic capture model that allows to design retrieval tools for magnetic cores of different diameters (down to 10 nm) and in different environmental conditions (fluid speed up to 7 cms^{-1}). The model robustness is demonstrated by the design and testing of a retrieval catheter. In its optimal configuration, the catheter includes 27 magnets and fits a 12 F catheter. The model provides a good prediction of capture efficiency for 250 nm magnetic particles (experimental data: 77.6%, model prediction: 65%) and a very good prediction for 500 nm particles (experimental data: 93.6%, model prediction: 94%). The results support the proposed model-based design approach, which can be extended to retrieve other magnetoresponsive agents from body compartments.

I. Introduction

Miniaturizing medical devices to get into the hard-to-reach areas of the human body and to perform localized targeted drug delivery, biopsy, surgery and diagnosis is one of the greatest challenges in medical robotics [1]. Such miniaturized tools, usually referred as micro- and nanorobots, hold the potential to reach body districts that cannot be accessed by traditional instruments.

To date, several strategies have been proposed for controlling micro and nanorobot locomotion by means of (*i*) externally applied magnetic [2, 3], acoustic [4] and light [5] fields, (*ii*) inclusion of biological motors [6, 7] or (*iii*) exploitation of chemical fuels [8]. Magnetic actuation has been deeply investigated in the state of the art with the aim to control microrobot locomotion across different body districts [9, 10]. Magnetic fields enable to safely and wirelessly control an object in a three-dimensional space and with multiple degrees of freedom, thus allowing it to follow complicated paths, if needed, to reach the target region [11, 12]. Despite significant advancements in the state of the art in terms of microrobots design and control strategies [13, 14], two main challenges still prevent the adoption of microrobots in the clinical practice [15]. The first is the inclusion in the control loop of a proper imaging modality suitable for tracking such tiny machines in the human body and control their position [16-18]. The second concerns safety: to become fully acceptable, microrobots should be either biodegradable or removed after task execution, to not raise short- and long-term side effects. Degradable and biocompatible materials have been proposed in microrobotics also combined with complex 3D fabrication techniques [19-21]. However, targeting an optimal compromise between magnetization (to enable control) and safety is not straightforward. Furthermore, the fate of the loaded therapeutic agents and of the inorganic nanoparticles or magnetic coatings should be considered when pursuing microrobot degradability as a solution.

The problem of microrobot retrieval has been scarcely approached in the literature. Some groups reported on the possibility to control microrobots in reverse motion [22] to potentially return from the target location upon task execution. However, this approach appears not feasible when dealing with microrobots featured by dimensions down to few tens of μm or nm. Physical laws scaling, fluid force balancing (especially when steering the microrobots against the blood flow) and difficulties in accurately controlling single microrobots (especially when dealing with large swarms) make this approach challenging.

Leveraging the above open issues on medical microrobots, in this paper the authors propose a model for capturing magnetic agents in the bloodstream. Once defined the microrobot features, in terms of magnetic properties, shape and hydrodynamic radius, and once defined blood vessels diameter and flow rate, the model permits to design a specific magnetic catheter for removing magnetic micro- and nanorobots from the bloodstream. The remainder of the paper is organized as follows. Section II describes the capture model, the numerical model built to study retrieval efficiency and the derived retrieval tool design. Section III describes the simulation results and the in vitro validation results. Finally, in section IV conclusion are drawn and the impact of the proposed retrieval model in the microrobotics field is highlighted.

* This work has been supported by the ROBO-IMPLANT project, funded by Tuscany Region (PAR FAS 2007-2013, Bando FAS Salute 2014) http://www.robo-implant.com

Dr. Veronica Iacovacci, Prof. Leonardo Ricotti and Prof. Arianna Menciassi are with the BioRobotics Institute, Scuola Superiore Sant'Anna, Pisa, Italy (email: veronica.iacovacci@santannapisa.it)

Dr. E. Sinibaldi is with the Center for Micro-BioRobotics @SSSA, Istituto Italiano di Tecnologia, Pontedera (PI), Italy

Dr. G. Signore is with Scuola Normale Superiore and Center for Nanotechnology Innovation @NEST, Istituto Italiano di Tecnologia, Pisa, Italy

Prof. F. Vistoli is with the Division of Transplantations Surgery, University of Pisa, Pisa, Italy

II. MAGNETIC MICROROBOT CAPTURE MODELING

A. Capture of magnetic micro- and nanorobots

In order to properly design a retrieval tool for specific magnetic microrobots, a capture modeling phase was tackled. From a physical viewpoint, the problem to be modeled consists of a magnetic micro-object dragged by a fluid (blood) that can be somehow deviated from its trajectory by means of a magnetic force (exerted by the retrieval tool). A peculiar aspect of our study is the fact that the intravascular magnetic sources strongly affect the carrying flow field.

The dynamics of a magnetic micro-object dragged by a fluid and immersed in a magnetic field can vary when considering complex microrobot geometries or locomotion strategies [23, 24]. However, based on size considerations, a point-dipole approximation can be reasonably applied to a variety of such micro-objects. From a geometrical viewpoint, microrobots were modeled as spherical, both to simplify the calculation of the drag force in the proposed model and because spherical drug carriers represent an important class of therapeutic microrobots. Based on these assumptions, the speed of a particle (v_p) dragged by a fluid with speed v and subject to a magnetic field H, results from the superposition of two contributions produced by fluid flow and magnetophoretic force, respectively. v_p can be thus expressed as follows:

$$v_p = v + \zeta f(H)(H \cdot \nabla)H \tag{1}$$

where ζ is the combination of drag and magnetic force acting on the particle (2), whereas *f(H)* is defined in (3) and expresses the contribution of microrobot magnetization and saturation due to the applied magnetic field.

$$\zeta = \frac{\mu_0(1+\chi_f)}{6\pi\eta_f}\frac{V_{mag}}{r_h} \tag{2}$$

$$f(H) = \begin{cases} \frac{3(\chi_p-\chi_f)}{(\chi_p-\chi_f)+3(1+\chi_f)} & \frac{M_{sp}}{H} > \frac{3(\chi_p-\chi_f)}{(\chi_p-\chi_f)+3(1+\chi_f)} \\ \frac{M_{sp}}{H} & \frac{M_{sp}}{H} \leq \frac{3(\chi_p-\chi_f)}{(\chi_p-\chi_f)+3(1+\chi_f)} \end{cases} \tag{3}$$

In the previous equations μ_0 is the magnetic vacuum permeability, χ_f and χ_p are the magnetic susceptibility of fluid and particles, respectively, η_f is the fluid dynamic viscosity, V_{mag} the volume of the magnetic core, M_{sp} the saturation magnetization, whereas r_h represents the particle hydrodynamic radius.

Essentially, designing a magnetic retrieval system means devising a magnetic field distribution enabling to counterbalance the fluid drag force and to properly deviate the micro-object from its trajectory, thus enabling its capture. At a first look to (1-3), some considerations on system behavior can be derived. For example, magnetophoresis contribution becomes dominant when magnetic core volume increases. On the other hand, a larger hydrodynamic radius favors particle dragging. It is also evident that to make the magnetophoretic contribution predominant, it is necessary to maximize the related field effects (reducing to gradient effects upon particle saturation). This should be a leading specification when designing the magnetic field source appointed for microrobots capture.

B. From the model to the retrieval catheter design

The capture of low volume particles dragged by a high speed flow is challenging and has been solved in different fields ranging from water purification [25] to magnetic separation systems for biological applications [26]. Usually, filter-like structures and/or huge magnetic field generation apparatuses are employed to produce magnetic forces sufficient to overcome the flow drag. However, the integration of such magnetic separation systems in a medical device is not straightforward due to dimensional constraints, biocompatibility issues and need of compliance with the bloodstream in the target scenario. In most works related to microrobots for medical applications, microrobot locomotion and dynamics are studied in capillaries, where flow rate is extremely reduced and steady-state assumptions can be made. On the other hand, when considering realistic working scenarios and body districts featured by large flow rate (e.g. about 30 cm/s as in the carotid [27]), few magnetic micro-objects can be stopped by external magnetic fields, although generated at small distances [28]. In order to obtain an effective retrieval through intravascular magnetic sources, it is also necessary to optimize their location in order to favorably condition the resulting flow field (this typically translates to a local decrease in speed where capture is sought).

Based on the capture model, the authors designed an intravascular tool able to canalize the blood, filter it from magnetic microrobots and reinsert the "clean blood" in the bloodstream (Figure 1). The catheter – like tool is modular: the magnetic retrieval module is the key part of the system; a tip balloon and a reinsertion module complete the tool design. An operating channel passes through the catheter for guidewire insertion, thus allowing the desired catheter positioning. The balloon enables to anchor the catheter to the vessel wall and to convey all the blood in the retrieval catheter. The magnetic module, in turn, enables to deviate magnetic microrobots from their trajectories and to remove them from the stream. Last, the reinsertion module, consisting of a series of openings in the catheter wall, enables filtered blood reinsertion into the bloodstream.

The capture catheter results particularly suitable for organs featured by terminal circulation, i.e. having a main arterial inlet and a main venous outlet, such as liver, kidneys, lungs and pancreas. In those districts in fact, the catheter can be placed in one of the main vein exiting the target organ where microrobot-mediated therapy has been performed. Microrobots could be injected at arterial level, as close as possible to the target organ.

Due to the high flow rates in realistic bloodstreams (not confined to capillary flows), the retrieval tools must be able to generate suitable magnetic fields to properly bend the flow streamlines and catch the microrobots. From (3) we can derive that for high-enough fields the particles saturate and the magnetic link is maximized where larger gradients occur. This suggested using miniature ring-shaped permanent magnets that, besides allowing for guidewire passage, easily provide high gradients close to their edges. Hence, particle capture was most probably expected at the edges rather that along the magnet body, thus making magnets height less relevant than radius (which, conversely, strongly affects the flow field because of cross-section reduction). As a consequence, the magnetic module was designed to include short permanent magnets consecutively stacked and separated by non magnetic spacers.

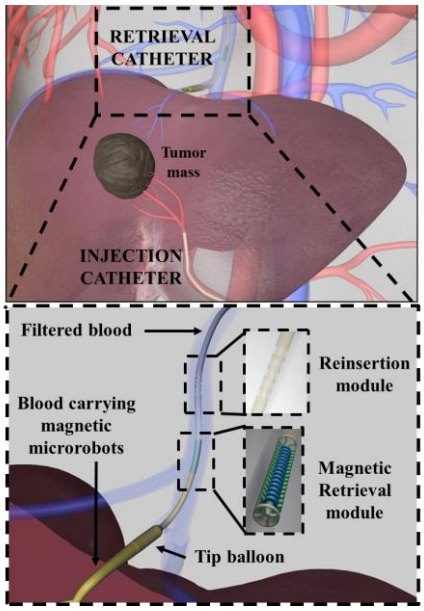

Figure 1 Modular retrieval catheter depiction in the liver and expanded view including the constitutive modules.

Furthermore, with the aim to maximize capture efficiency while preserving module compactness, the magnetic module was designed to include two coaxial sets of permanent magnets (internal and external sets) (Figure 2), connected at both ends. Connection elements included proper fenestrations to enable blood flow; they allowed anchoring the magnetic module to the catheter structure while keeping the two coaxial sets of magnets together.

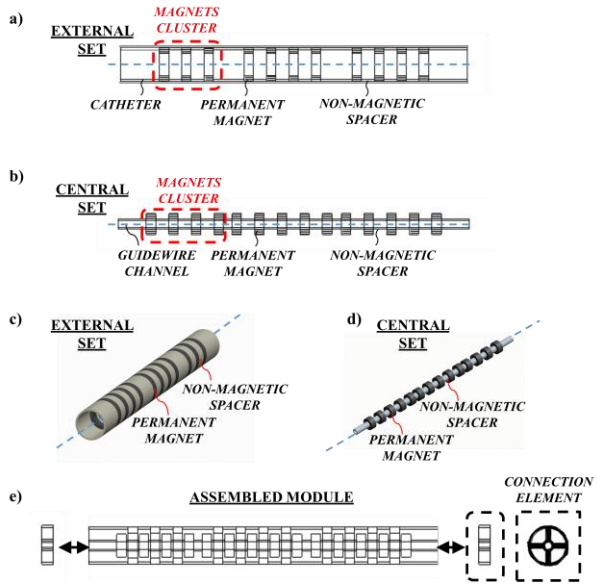

Figure 2 Magnetic module schematization. a-d) External and central set of magnets (2D and 3D views). The symmetry axis is drawn in blue. e) Module assembly.

C. *FEM modeling*

Finite Element Method (FEM) simulations enabled to evaluate capture module performances when varying magnets size, number and spatial arrangement, particles dimension and blood velocity. Magnetic microrobots dragged by the bloodstream and passing through the magnetic catheter were modeled as magnetic particles (point dipoles); we assumed the hydrodynamic radius to coincide with that of the magnetic core, for simplicity. Thanks to a tip balloon, the blood is canalized toward the magnetic module inlet. We thus considered a confined laminar flow [28] carrying magnetoresponsive agents, and we assumed a one-way coupling (the particle presence did not affect the flow). A non-trivial design problem emerged: narrowing the blood passages to get closer to the particles, as functional for magnetic capture, systematically implies flow acceleration, which is clearly detrimental for magnetic capture. FEM simulations aimed at identifying a suitable trade-off (i.e. optimized gap) to solve the aforementioned problem.

A FEM model was built in Comsol Multiphysics® environment (Comsol Group, Stockholm, Sweden). It included two stationary studies: one for the magnetic field (Magnetic Fields – no Current Module in Comsol Multyphysics®), the other one for the laminar flow (Laminar Flow Module in Comsol Multyphysics®). Particle trajectories were then reconstructed (Particle Tracing Module in Comsol Multyphysics®). In implementing the particle tracing, the force field obtained by magnetic and fluidic modeling solutions were imported to define the drag force and magnetophoresis actions on the magnetic particles. In order to avoid a huge computational burden especially when increasing magnet number and geometrical complexity, 2D axial-symmetric simulations were performed exploiting the degree of symmetry introduced by a cylindrical geometry. An extremely fine triangular custom mesh (10 µm element size in the flow region and 50 µm element size elsewhere) was built and mesh-independence was assessed through preliminary runs.

We designed the magnets arrangement based on FEM simulations, namely to obtain an optimal capture efficiency. Capture efficiency represents the ratio between the number of particles captured by the magnetic module and the injected one. Simulation were performed at varying magnet dimensions, number, arrangement (including possible clustering), particle dimensions and fluid speed. All parameters are summarized in Table I. As a first step, the effect on retrieval efficiency of a single magnet placed either at the center or on the external wall of the module was assessed. Particle trajectories were then computed for an increasing number of magnets arranged according to the two coaxial sets configuration described above and organized in clusters (Figure 2). Indeed, given a fixed number of magnets, the efficiency is affected by their spatial distribution, namely their clusters. More precisely, the gap between clusters brings a penalization in terms of total length of the module, yet it allows to decrease the fluid speed entering each cluster (because of trivial mass conservation arguments). This effect brings a potential benefit for capture. In this framework, magnets clustering resulted by a design trade-off. In order to fix some dimensions and to reduce the computational time, two magnetic module external diameter values were fixed, namely 3.6 and 4.6 mm. These diameters guarantee compliance with a 12F and 15F catheter, respectively. Both configurations were provided with a 1mm central channel for the guidewire passage.

Magnetic module	External Diameter 3.6 – 4.9 mm	Internal Channel 1 mm	Length 1 - 40 mm
Working fluid (blood)	Dynamic Viscosity 35 Cp	Density 1035 kg· m^{-3}	Speed 0 - 7 cm· s^{-1}
Permanent Magnets	Grade N52 (axial magnetization)	Height 0.8 - 2 mm	Wall Thickness 0.6 – 1 mm
Magnetic particles	Diameter 10 - 500 nm	Relative magnetic permeability 10^3	

Table 1 Magnetic capture modeling parameters.

Retrieval efficiency was evaluated also for different particles dimensions (10–500 nm) and blood speed values (0–7 cms^{-1}) in order to investigate potential employment in different body districts featured by a different fluid dynamics. The liver was considered as a case study and blood velocity in the supra-hepatic vein (7 cms^{-1}) was taken as reference parameter.

D. Magnetic module prototyping and retrieval testing

Permanent magnets and 3D printed spacers (wall thickness 200 µm and external diameter equal to that of the adjacent permanent magnet) were alternately stacked according to the optimal configuration derived from simulations to form the central and external sets. The coaxial sets were then assembled together by means of 3D printed connection elements and embedded in a thermoplastic structure. Bi-stable heat-shrinkable fluorinated ethylene propylene (FEP) extruded tubes (ZEUS, USA) featured by a transition temperature around 215°C, were employed to this aim. The thermally triggered bi-stability of this product allowed an easy magnetic module encapsulation without implying neither a significant alteration of the diameter (tube wall thickness was 100 µm) nor compromising module integrity or requiring complex assembly procedures (Figure 3).

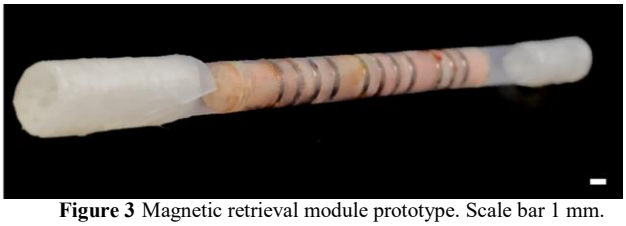

Figure 3 Magnetic retrieval module prototype. Scale bar 1 mm.

In vitro validation was carried out with the aim to evaluate the accuracy of the proposed FEM model and to evaluate the magnetic retrieval efficiency of the designed magnetic module. A dedicated test bench including a fluidic micropump (M100 series, TCS), the magnetic retrieval module and a controller allowing samples collection, was designed and fabricated (Figure 4). In order to mimic blood fluid dynamics, a blood resembling water-glycerol solution (42% v/v in water [29]) was employed as working fluid and the pumping device was properly calibrated and driven to reproduce the simulated blood speed.

Retrieval tests were performed by injecting 100 µL bolus of magnetic particles and by collecting a 30 mL sample of the fluid exiting from the magnetic module. On the other hand, the particles injection point was selected far enough from the magnetic capture module, to enable mixing between the working fluid and the magnetic particle dispersion medium, thus a proper distribution of the particles in the fluid profile. In order to quantify the capture efficiency, the samples collected at the circuit output were analyzed through Inductively Coupled Plasma Mass Spectrometry (ICP-MS). This technique enabled to quantify the amount of nanoparticles dispersed in the sample, thus not retrieved by the magnetic module. Samples underwent sonication, dissolution in hydrochloric acid, digestion and dilution (Agilent Technologies 7700 Series ICP-MS) [30] prior measurements. By assuming a uniform distribution of nanoparticles in the collected volume, the amount of iron (thus of nanoparticles) was derived (by comparison with a standard curve). Capture efficiency was calculated by correlating the amount of iron in the collected samples with the injected one.

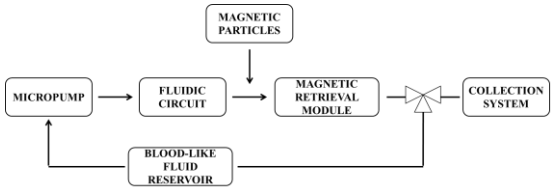

Figure 4 In vitro testing fluidic circuit schematics.

The capture model was validated through two testing runs. At a first stage, 4.9 mm diameter module prototypes were fabricated from off-the-shelf components. Despite this was not an optimized design, preliminary assessment enabled to test the experimental protocol besides model predictive capabilities. A more extensive set of tests was then performed on twelve magnetic module prototypes fabricated according to the optimal configuration derived from simulations (employing custom magnets), by following the same experimental protocol and by considering two different particle diameters (250 nm and 500 nm, 09-01-252 and 09-01-502, Micromod, Germany).

III. RESULTS

A. FEM retrieval modeling

From the first simulations, it was clear that by exploiting a single magnet set, either placed at the center of the vessel or along the side wall (external), it would be practically impossible to achieve high particle capture efficiency. Due to obstacle presence, the majority of the particle will tend to flow far from the permanent magnets thus minimizing the amount of particles subject to magnetic attraction force and consequently capture efficiency. When considering a single ring-shaped magnet, 500 nm nanoparticles capture efficiency varied from 38% to 20% when placing the magnet along the side wall (d_{ext}=3.6 mm, d_{int}=2.4 mm, h=1 mm) or at the center of the vessel (d_{ext}=2.2 mm, d_{int}=1 mm, h=1 mm), respectively.

On the other hand, by exploiting two coaxial sets of ring-shaped magnets, particles are constrained to a "wavy trajectory" along the gap between the two magnet sets. Tightening the gap caused a significant increase in particles speed. At the same time, due to magnetic gradients effect at magnet edges, small gaps maximized capture efficiency: a tradeoff between these two effects should be identified, which

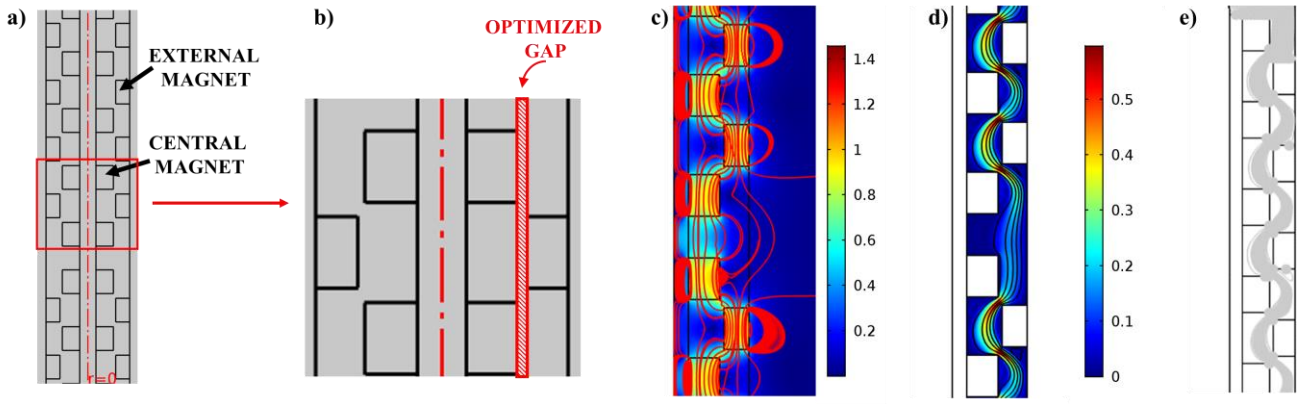

Figure 5 Multiphysics simulation results. a) Magnetic module 2D representation in COMSOL Multiphysics environment; b) zoomed view of a portion of the magnetic module; c–e) Fluidic velocity [ms^{-1}], magnetic field [T], and particle trajectories (100 particles were considered) in the proposed magnetic module.

corresponded to the optimized gap. A typical depiction of the proposed FEM model is reported in Figure 5where the fluidic and magnetic fields, as well as particles trajectories in a sagittal cut-section of the proposed magnetic module are represented.

Simulation results by varying the number of magnets included in both 3.6 and 4.6 mm overall diameter modules are reported in Figure 6. All the reported data were calculated while considering 500 nm magnetic particles. For both module sizes, retrieval efficiency increased with magnets number but with a slower trend for configurations including more than 14 magnets, thus suggesting the reaching of a sort of plateau for larger modules. Simulation results revealed a retrieval efficiency up to 89% and 92% for 27 magnets in 4.6 and 3.6 mm module, respectively.

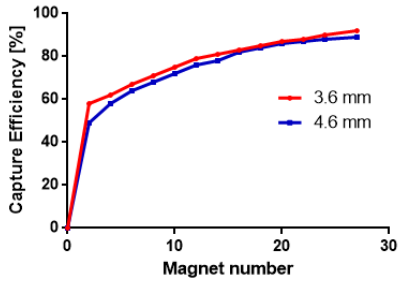

Figure 6 FEM simulations results in terms of capture efficiency when varying magnets number and module diameter (500 nm nominal diameter particles and a fluid speed of 7cms^{-1} were considered).

Reduced module caliber resulted in better retrieval performances due to a more efficient equilibrium between gap size and force balance. Once fixed magnets dimensions accordingly (external set - $d_{ext.}$=3.6 mm – d_{int}=2.4 mm – h=1 mm and central set - $d_{ext.}$=2.2 mm – d_{int}=1 mm – h=1 mm) and once considered a fixed overall magnets number equal to 27, simulations revealed also the contribution played by magnets clustering (Figure 7). In the best configuration, magnets are organized in three clusters for an overall module length of 33.7 mm. 94% of the 500 nm injected particles can be retrieved by the magnetic capture module in this configuration.

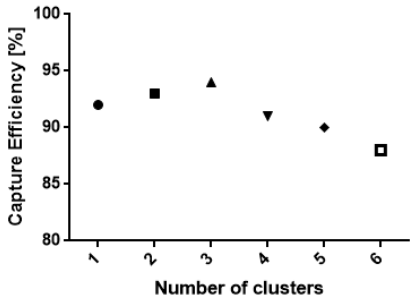

Figure 7 FEM simulations results in terms of capture efficiency when varying the clustering of 27 magnets (500 nm nominal diameter particles and a fluid speed of 7cms^{-1} were considered).

As expected, retrieval efficiency exponentially drops when reducing magnetic core diameter. However, 18% capture efficiency is achieved when dealing with particle diameters as small as 10 nm (Figure 8), suggesting to consider the intravascular tool at hand for nanorobotics and nanomedicine applications.

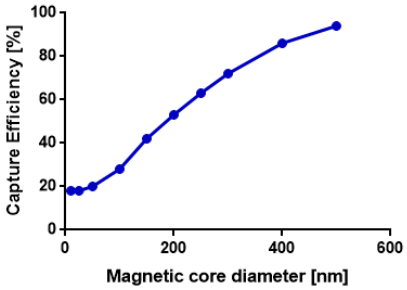

Figure 8 FEM simulations results in terms of capture efficiency when varying magnetic core diameter (fluid speed of 7cms^{-1}).

Lastly, simulations performed by considering the magnetic module optimal configuration and 500 nm particles revealed that the devised system is theoretically able to reach a 100% capture efficiency for blood speed below 3.5 cms^{-1} (Figure 9). This result paves the way to the employment of the proposed tool also in other body districts (different from the liver) and in blood vessels featured by different speeds.

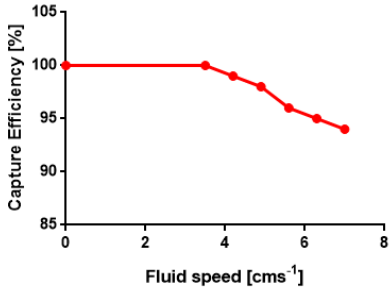

Figure 9 FEM simulations results in terms of capture efficiency when varying blood speed (500 nm nominal diameter particles and a fluid speed of 7cms^{-1} were considered).

B. *In vitro retrieval testing*

Retrieval tests were preliminarily carried out on a 4.9 mm prototype (external set - d_{ext}=4.9 mm – $d_{int.}$=2.9 mm – h=2 mm and central set - $d_{ext.}$=2.5 mm – $d_{int.}$=1 mm – h 0.8 mm) fabricated from off-the-shelf components. In its design, geometrical and dimensional proportions among constitutive components were kept fixed with respect to the final configuration selected through simulations.

In vitro validation was performed through the described fluidic circuit (fluid speed 7cms^{-1}) and by injecting a 100 µL bolus of 500 nm magnetic nanoparticles. Multiple tests were performed on two prototypes revealing a 75% (average) capture efficiency against a theoretical efficiency of 84% (evaluated by including in the model the geometrical and residual magnetization features of the embedded magnets).

A more extensive set of tests was then performed on magnetic module prototypes fabricated according to the optimal configuration (3.6 mm external diameter) derived from simulations, by following the same experimental protocol. In this case, the prototype included 27 permanent magnets organized in three clusters (Figure 7 and Figure 3). The mismatch between theoretical (FEM) and experimental retrieval efficiency, corresponding to 94% and 93.6% respectively, was minimal revealing an optimal capability of the model to predict system behavior (Figure 10).

Capture efficiency was evaluated also with smaller nanoparticles, showing a 250 nm nominal diameter. ICP-MS analysis on the collected samples revealed a capture efficiency equal to 77.6% against the 65% capture efficiency predicted through FEM simulations. Despite the discrepancy between theoretical and experimental efficiency is larger in this case if compared to tests performed with 500 nm particles, the capability of the model to predict system behavior is confirmed.

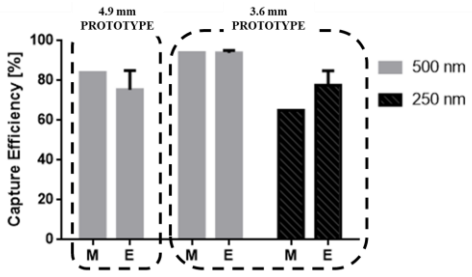

Figure 10 Comparison among theoretical (calculated through FEM - M) and experimental (E) capture efficiency when considering two module size and 500 and 250 nm magnetic particles.

IV. Conclusion

In this paper, the authors proposed a novel paradigm for magnetic microrobots retrieval. The developed capture model enabled to design a magnetic retrieval module suitable for inclusion in a 12F modular catheter and enabling to reach ≈ 94% retrieval efficiency. In vitro validation revealed that the proposed design is suitable for the devised application and that the developed FEM model represents a reliable tool to guide system design towards the development of a real biomedical device. Focusing on a single test-case, namely liver applications, the authors recently reported that the magnetic module does not alter key blood characteristics and that retrieval efficiency is not altered when considering repeated capture runs, thus supporting its potential for effective exploitation [31]. By changing few parameters (hydrodynamic radius and magnetization) the model can be employed to predict the retrieval efficiency of state of the art microrobots. In this framework, the proposed capture model represents a valid tool in the field of microrobotics for medical application since paving the way to an effective retrieval of magnetic microrobots.

Acknowledgment

This work has been supported by the ROBO-IMPLANT project, funded by Tuscany Region (PAR FAS 2007-2013, Bando FAS Salute 2014) http://www.robo-implant.com.

References

[1] H. Ceylan, J. Giltinan, K. Kozielski, and M. Sitti, "Mobile microrobots for bioengineering applications," *Lab on a Chip,* vol. 17, pp. 1705-1724, 2017.

[2] J. Rahmer, C. Stehning, and B. Gleich, "Spatially selective remote magnetic actuation of identical helical micromachines," *Science Robotics,* vol. 2, no. 3, p. eaal2845, 2017.

[3] G. Lucarini, V. Iacovacci, L. Ricotti, N. Comisso, P. Dario, and A. Menciassi, "Magnetically driven microrobotic system for cancer cell manipulation," in *Engineering in Medicine and Biology Society (EMBC), 2015 37th Annual International Conference of the IEEE*, 2015, pp. 3631-3634.

[4] D. Ahmed, T. Baasch, B. Jang, S. Pane, J. r. Dual, and B. J. Nelson, "Artificial swimmers propelled by acoustically activated flagella," *Nano Letters,* vol. 16, pp. 4968-4974, 2016.

[5] S. Palagi, A. G. Mark, S. Y. Reigh, K. Melde, T. Qiu, H. Zeng, *et al.*, "Structured light enables biomimetic swimming and versatile locomotion of photoresponsive soft microrobots," *Nature materials,* vol. 15, pp. 647–653, 2016.

[6] D. De Lanauze, O. Felfoul, J.-P. Turcot, M. Mohammadi, and S. Martel, "Three-dimensional remote aggregation and steering of magnetotactic bacteria microrobots for drug delivery applications," *The International Journal of Robotics Research,* vol. 33, pp. 359-374, 2014.

[7] L. Ricotti, B. Trimmer, A. W. Feinberg, R. Raman, K. K. Parker, R. Bashir, *et al.*, "Biohybrid actuators for robotics: A review of devices actuated by living cells," *Sci. Robot.,* vol. 2, p. eaaq0495, 2017.

[8] J. Li, P. Angsantikul, W. Liu, B. Esteban- Fernández de Ávila, S. Thamphiwatana, M. Xu, *et al.*, "Micromotors Spontaneously Neutralize Gastric Acid for pH- Responsive Payload Release," *Angewandte Chemie International Edition,* vol. 56, pp. 2156-2161, 2017.

[9] V. Iacovacci, G. Lucarini, L. Ricotti, P. Dario, P. E. Dupont, and A. Menciassi, "Untethered magnetic millirobot for targeted drug delivery," *Biomedical microdevices,* vol. 17, p. 63, 2015.

[10] S. Martel, "Targeting active cancer cells with smart bullets," *Therapeutic delivery,* vol. 8, no. 5, pp. 301-312, 2017.

[11] E. Diller, J. Giltinan, and M. Sitti, "Independent control of multiple magnetic microrobots in three dimensions," *The International Journal of Robotics Research,* vol. 32, pp. 614-631, 2013.

[12] B. E. Kratochvil, M. P. Kummer, S. Erni, R. Borer, D. R. Frutiger, S. Schürle*, et al.*, "MiniMag: a hemispherical electromagnetic system for 5-DOF wireless micromanipulation," in *Experimental Robotics*, pp. 317-329, 2014.

[13] S. Martel, M. Mohammadi, O. Felfoul, Z. Lu, and P. Pouponneau, "Flagellated magnetotactic bacteria as controlled MRI-trackable propulsion and steering systems for medical nanorobots operating in the human microvasculature," *The International journal of robotics research,* vol. 28, pp. 571-582, 2009.

[14] A. Oulmas, N. Andreff, and S. Régnier, "3D closed-loop motion control of swimmer with flexible flagella at low Reynolds numbers," in *Intelligent Robots and Systems (IROS), 2017 IEEE/RSJ International Conference on*, 2017, pp. 1877-1882.

[15] M. Medina-Sánchez and O. G. Schmidt, "Medical microbots need better imaging and control," *Nature,* vol. 545, p. 25, 2017.

[16] X. Yan, Q. Zhou, M. Vincent, Y. Deng, J. Yu, J. Xu*, et al.*, "Multifunctional biohybrid magnetite microrobots for imaging-guided therapy," *Sci. Robot,* vol. 2, no. 12, p. eaaq1155, 2017.

[17] D. Vilela, U. Cossío, J. Parmar, A. M. Martínez-Villacorta, V. Gómez-Vallejo, J. Llop*, et al.*, "Medical Imaging for the Tracking of Micromotors," *ACS nano,* vol. 12, pp. 1220-1227, 2018.

[18] S. Pané, J. Puigmartí- Luis, C. Bergeles, X. Z. Chen, E. Pellicer, J. Sort*, et al.*, "Imaging Technologies for Biomedical Micro- and Nanoswimmers," *Advanced Materials Technologies,* 1800575, 2019.

[19] H. Ceylan, I. C. Yasa, O. Yasa, A. F. Tabak, J. Giltinan, and M. Sitti, "3D-Printed Biodegradable Microswimmer for Drug Delivery and Targeted Cell Labeling," *bioRxiv,* p. 379024, 2018.

[20] C. Peters, M. Hoop, S. Pané, B. J. Nelson, and C. Hierold, "Degradable Magnetic Composites for Minimally Invasive Interventions: Device Fabrication, Targeted Drug Delivery, and Cytotoxicity Tests," *Advanced Materials,* vol. 28, pp. 533-538, 2016.

[21] X. Wang, X. H. Qin, C. Hu, A. Terzopoulou, X. Z. Chen, T. Y. Huang*, et al.*, "3D Printed Enzymatically Biodegradable Soft Helical Microswimmers," *Advanced Functional Materials,* p. 1804107, 2018.

[22] H.-W. Huang, M. S. Sakar, A. J. Petruska, S. Pané, and B. J. Nelson, "Soft micromachines with programmable motility and morphology," *Nature Communications,* vol. 7, p. 12263, 2016.

[23] H. W. Huang, Q. Chao, M. S. Sakar, and B. J. Nelson, "Optimization of Tail Geometry for the Propulsion of Soft Microrobots," *IEEE Robotics and Automation Letters,* vol. 2, pp. 727-732, 2017.

[24] I. S. Khalil, H. C. Dijkslag, L. Abelmann, and S. Misra, "MagnetoSperm: A microrobot that navigates using weak magnetic fields," *Applied Physics Letters,* vol. 104, p. 223701, 2014.

[25] R. D. Ambashta and M. Sillanpää, "Water purification using magnetic assistance: A review," *Journal of Hazardous Materials,* vol. 180, pp. 38-49, 2010.

[26] D. W. Inglis, R. Riehn, J. C. Sturm, and R. H. Austin, "Microfluidic high gradient magnetic cell separation," *Journal of Applied Physics,* vol. 99, p. 08K101, 2006.

[27] B. J. Nelson, I. K. Kaliakatsos, and J. J. Abbott, "Microrobots for minimally invasive medicine," *Annual review of biomedical engineering,* vol. 12, pp. 55-85, 2010.

[28] L. C. Berselli, P. Miloro, A. Menciassi, and E. Sinibaldi, "Exact solution to the inverse Womersley problem for pulsatile flows in cylindrical vessels, with application to magnetic particle targeting," *Applied Mathematics and Computation,* vol. 219, pp. 5717-5729, 2013.

[29] P. Hoskins, T. Loupas, and W. McDicken, "A comparison of the Doppler spectra from human blood and artificial blood used in a flow phantom," *Ultrasound in medicine & biology,* vol. 16, pp. 141-147, 1990.

[30] L. Ricotti, G. Gori, D. Cei, J. Costa, G. Signore, and A. Ahluwalia, "Polymeric microporous nanofilms as smart platforms for in vitro assessment of nanoparticle translocation and Caco-2 cell culture," *IEEE transactions on nanobioscience,* vol. 15, pp. 689-696, 2016.

[31] V. Iacovacci, L. Ricotti, E. Sinibaldi, G. Signore, F. Vistoli, and A. Menciassi, "An Intravascular Magnetic Catheter Enables the Retrieval of Nanoagents from the Bloodstream," *Advanced Science,* 1800807, 2018.